ISSN 1560-8034, 1605-6582 (On-line), SPQEO, 2019. V. 22, N 4. P. 397-403.

Conduction mechanisms of the reverse leakage current of β-Ga_2O_3 Schottky barrier diodes

A. Latreche

Département des sciences de la matière, Université de Bordj Bou Arreridj,
34000, Algeria
E-mail: hlat26@ yahoo.fr.

Abstract. In order to determine the temperature dependence of the reverse transition voltage between thermionic emission and tunneling mechanisms, a numerical method has been applied for β-Ga_2O_3 Schottky barrier diodes. The main idea of this method is based on the intersection of *I–V* curves of thermionic emission and tunneling process. The reverse transition voltage increases for low and high temperatures, while it decreases at intermediate temperatures. This means that unexpected peak by Padovani–Stratton's condition is observed at low temperatures. The reverse transition voltage increases linearly with increasing the barrier height, and the inverse of doping concentration. An analytical model has been proposed to predict the dependence of the reverse transition voltage on temperature, doping concentration and barrier height for β-Ga_2O_3 Schottky barrier diodes. This model is well tested on experimental reverse transition voltage data previously published in the literature for β-Ga_2O_3 SBDs.

Keywords: β-Ga_2O_3, reverse transition voltage, thermionic emission, tunneling current, Schottky diode, image force barrier lowering.

https://doi.org/10.15407/spqeo22.04.397
PACS 85.30.De, 85.30.Kk, 85.30.Mn

Manuscript received 15.05.19; revised version received 10.06.19; accepted for publication 29.10.19; published online 08.11.19.

1. Introduction

The monoclinic beta-phase of gallium oxide (β-Ga_2O_3) becomes one of the most attractive materials in recent years, for next generation power electronic devices due to their excellent material properties for high voltage applications, *e.g.*, the breakdown field of 8 MV/cm, 4.8 eV bandgap, and Baliga's figure of merit that is more than 4 times larger than those for other wide bandgap materials GaN and SiC [1-7]. Moreover, β-Ga_2O_3 material is available as high-quality freestanding β-Ga_2O_3 substrates grown using the inexpensive melt methods [7]. The Schottky barrier diodes (SBDs) based on β-Ga_2O_3 material are being conducted early-stage research by several authors. Few studies have dealt with the electrical behavior of β-Ga_2O_3 SBDs using β-Ga_2O_3 single crystal grown using the several growth methods with different crystal orientations [8-25]. In these works, the most of the authors investigated the electrical conduction in β-Ga_2O_3 SBDs under forward bias conditions where the thermionic emission current dominates the forward total current. However, it is not yet clear which mechanism is dominant under reverse bias, and further attempts and investigations are undergoing to analyze and understand the origin of the undesirable large leakage currents that have been observed in the wide bandgap semiconductor SBDs such as SiC, GaN and β-Ga_2O_3, due to the high electric fields normally encountered at the metal/semiconductor interface. Higashiwaki *et al.* [12] investigated the reverse characteristics *I-V* of Pt/Ga_2O_3 (001) Schottky barrier diodes fabricated on *n*-Ga_2O_3 drift layers grown using the halide vapor phase epitaxy, in the operation temperature range from 21 to 200 °C at reverse bias voltages ranging from zero bias up to 200 V, they have found that the reverse leakage current agrees well with the thermionic field emission (TFE) model as would be expected of wide bandgap semiconductor SBDs. Konishi and his co-authors [18] investigated the reverse characteristics of vertical Ga_2O_3 FP-SBDs using an HVPE-grown drift layer fabricated on a Si-doped *n*-β-Ga_2O_3 drift layer grown using the halide vapor phase epitaxy on a Sn-doped *n*-Ga_2O_3 (001) substrate under the same conditions of temperature and reverse bias as Higashiwaki *et al.*

© 2019, V. Lashkaryov Institute of Semiconductor Physics, National Academy of Sciences of Ukraine

They concluded that the thermionic emission (TE) process dominates the current flow under both forward and reverse bias conditions. In our more recent theoretical and experimental works [26, 27], we investigated the conduction mechanisms of the leakage current for 4H-SiC SBDs and found that the reverse transition voltage versus temperature plot was strongly dependent on several parameters, namely: doping concentration, barrier height and effective mass. Since the electron effective mass in β-Ga_2O_3 material is different from that of 4H-SiC material, so, one can expect a significant change in the reverse transition voltage for β-Ga_2O_3 SBDs. In this work, due to the difficulty of obtaining a unified analytical expression of the reverse transition voltage as a function of temperature, doping concentration and barrier height for all types of Schottky diodes, we will also investigate the conduction mechanisms of the leakage current for β-Ga_2O_3 SBDs to identify the ranges of temperature and reverse bias, over which β-Ga_2O_3 Schottky diodes exhibit tunneling and thermionic emission, and propose another model to predict the reverse transition voltage as a function of temperature, doping concentration and barrier height for β-Ga_2O_3 SBDs. This model will be tested on experimental reverse transition voltage data previously published in the literature.

2. Theory and modeling

The total electron current density flowing through the Schottky barrier diode is the sum of the two dominant components, namely: thermionic emission over the potential barrier and carrier tunneling through the potential barrier [28]. The thermionic emission current density with including the image force lowering is expressed by [29]

$$J_{Therm} = A^* T^2 e^{-\frac{q}{k_B T}(\phi_b - \Delta\phi_b)}, \tag{1}$$

where T is the temperature, A^* – effective Richardson constant, k_B – Boltzmann constant, and the barrier lowering due to the image force effect is given by [30]:

$$\Delta\phi_b = \left[\frac{q^3 N_D (\phi_b - \varsigma - V_R)}{8\pi^2 \varepsilon_s^3}\right]^{1/4}, \tag{2}$$

where ε_s is the semiconductor permittivity, N_D – doping concentration, and ζ – distance between the conduction band and the equilibrium Fermi level.

The reverse leakage current of the Schottky barrier diode by tunneling process is expressed by [29, 31-34]

$$J_{Tun} = \frac{A^* T}{k_B} \int_0^{U_{max}} T(E_x) \ln\left(\frac{1 + \exp(-q\varsigma - E_x)/k_B T}{1 + \exp(-q\varsigma - qV_R - E_x)/k_B T}\right) dE_x. \tag{3}$$

Here, $T(E_x)$ is the tunneling probability calculated using the Wentzel–Kramers–Brillouin (WKB) approximation

$$T_{WKB}(E_x) = \exp\left[-2\int_{x_1}^{x_2}\left(\frac{2m^*}{\hbar^2}(U(x) - E_x)\right)^{1/2} dx\right], \tag{4}$$

where x_1 and x_2 are two classical turning points. The WKB approximation predicts tunneling current through a reverse biased Schottky barrier with credible accuracy [33]. Including the image force lowering effect, the potential energy profile $U(x)$, for an arbitrary Schottky diode as measured with respect to the energy of the bottom of the conduction band in the bulk of the semiconductor, it can be given by [29, 34]

$$U(x) = \frac{q^2 N_D}{2\varepsilon_s}(D - x)^2 - \frac{q^2}{16\pi\varepsilon_s x}, \tag{5}$$

where D is the depletion width dependent on the reverse bias voltage V_R.

By using the general expression (3) of the tunneling current and neglecting the image force lowering, Padovani and Stratton [35] analyzed tunneling currents in Schottky barriers from the standpoint of field emission (FE) and thermionic field emission (TFE) by using one-dimensional WKB approximation. Padovani and Stratton [35] developed their model by considering only the first three terms of the Taylor series expansion of the exponent of the transparency of the barrier around energy E_m above the bottom of the conduction band for the thermionic field emission model, and the first two terms of the Taylor series expansion of the exponent of the transparency of the barrier around the Fermi level for field emission model, and, therefore, there are restrictions that must be met to ensure accuracy.

In the intermediate temperature range, where thermionic field emission is dominant, the current density in the reverse direction is expressed by the following equation [35]:

$$J_{TFE} = \frac{A^* T}{k_B}\sqrt{\pi E_{00} q\left(-V + \frac{\phi_b}{\cosh^2(E_{00}/k_B T)}\right)} \times \exp\left(-\frac{q\phi_b}{E_0}\right)\exp\left(-\frac{qV}{\varepsilon'}\right), \tag{6}$$

where

$$\varepsilon' = \frac{E_{00}}{(E_{00}/k_B T) - \tanh(E_{00}/k_B T)}, \tag{7}$$

$$E_0 = E_{00}\coth(E_{00}/k_B T), \tag{8}$$

$$E_{00} = \frac{h}{4\pi}\left(\frac{N_D}{m^* \varepsilon_s}\right). \tag{9}$$

The condition which gives the upper temperature limit or the minimum bias to apply to the diode in order to observe thermionic-field emission is given by [35]

$$-V > \phi_b + \frac{3E_{00}}{2q} \frac{\cosh^2(E_{00}/k_B T)}{\sinh^3(E_{00}/k_B T)} . \quad (10)$$

If the temperature gets lower or the reverse bias gets higher the current is dominated by pure field emission, which can be expressed as [35]

$$J_{FE} = \frac{A^* T^2 \pi E_{00} \exp\left[-2q\phi_b^{3/2} / 3E_{00}(\phi_b - V)^{1/2}\right]}{k_B T [\phi_b/(\phi_b - V)]^{1/2} \sin\left\{\pi k_B T [\phi_b/(\phi_b - V)]^{1/2} / E_{00}\right\}} . \quad (11)$$

The transition between thermionic field emission (TFE) and field emission (FE) is given by the constant c_1, where

$$\begin{cases} 1/c_1 < k_B T, & \text{for TFE}, \\ 1/c_1 > k_B T, & \text{for FE}. \end{cases} \quad (12)$$

The constant c_1 is given for reverse biases in such a manner that $-V > \phi_b$ by

$$c_1 = E_{00}^{-1} [\phi_b/(\phi_b - V)]^{1/2} . \quad (13)$$

In our recent study [36], we tested the accuracy of the Padovani–Stratton model (Eqs. (6) and (11)) in terms of the percent error in the barrier height over a range – 1000 V at room temperature with and without the image force barrier lowering. We found that Padovani–Stratton model is less accurate when the image barrier lowering is ignored at low reverse bias voltage, however, it is inaccurate when we take into account the image barrier lowering on entire range bias.

3. Results and discussion

The parameters chosen for performing the simulation of reverse characteristics *I-V* of β-Ga_2O_3 Schottky barrier diode are: effective mass $m^* = 0.342m_0$ [37], theoretical effective Richardson constant $A^* = 41.1\ \text{A cm}^{-2}\cdot\text{K}^{-2}$, semiconductor permittivity $\varepsilon_s = 10.2\varepsilon_0$ [38, 39] and $\phi_b = 1.1$ eV. The calculated reverse current densities according to tunneling and thermionic emission models for β-Ga_2O_3 Schottky barrier diode at room temperature with doping concentration $N_D = 5.10^{15}\ \text{cm}^{-3}$, barrier height $\phi_b = 1.1$ eV and effective mass $m^* = 0.342m_0$ are shown in Fig. 1. The calculation includes the effect of image force lowering in both the thermionic emission and electron tunneling process. As shown in this figure, the total *I-V* characteristic is the result of two current components: the tunneling current, and the thermionic emission current. As shown in Fig. 1, both generated curves $(I\text{-}V)_{Tun}$ and $(I\text{-}V)_{Therm}$ are intersected. The intersection voltage is the reverse transition voltage (V_T) between thermionic emission and tunneling mechanisms.

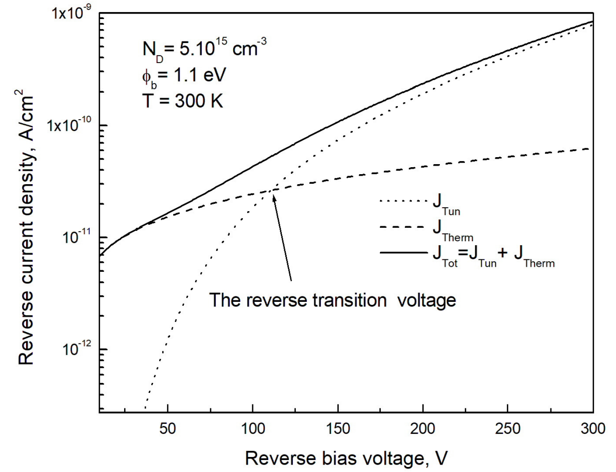

Fig. 1. Reverse *I-V* characteristics based on both the thermionic emission and tunneling processes for β-Ga_2O_3 SBD.

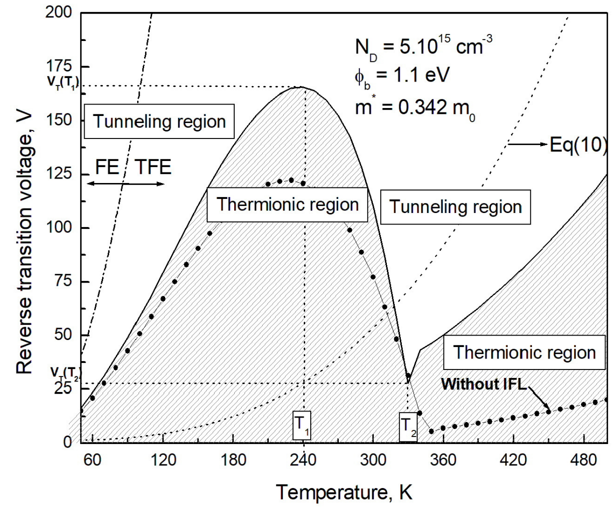

Fig. 2. Ranges of temperature and reverse bias, over which β-Ga_2O_3 Schottky diodes exhibit tunneling and thermionic emission in the case when the image force lowering is included. Comparison with Padovani–Stratton's condition.

As shown in Fig. 1, the transition between thermionic emission and tunneling occurs at approximately V_T = = 111 V reverse bias. For a high bias (V >> 111 V) the total current is dominated by the tunneling current, while at low reverse bias (V << 111 V) the thermionic emission current becomes the dominant one. Near the reverse transition voltage, neither tunneling nor thermionic emission accurately describes the conduction process because both these currents have the same order of magnitude, therefore, both mechanisms should be combined together.

The intersection between the generated curves *I-V* for a given temperature determines the ranges of temperatures and reverse bias over which β-Ga_2O_3 Schottky barriers exhibit tunneling and thermionic emission as shown in Fig. 2 with $N_D = 5.10^{15}\ \text{cm}^{-3}$, barrier

height $\phi_b = 1.1$ eV and effective mass $m^* = 0.342m_0$. For comparison, we also show the ranges of temperature and reverse bias obtained without image force lowering (IFL) by using our method (Eqs. (1) and (3) without inclusion of image force lowering) and by using the Padovani–Stratton condition given by Eq. (10). As shown in Fig. 2, the reverse transition voltage increases for low (< 240 K) and high (> 330 K) temperatures with increasing temperature, while it decreases with increasing temperature in the intermediate temperature range (240…330 K).

The competition between both these mechanisms, thermionic emission and tunneling, makes in the curve two local extrema points: a local maximum point at approximately $T_1 = 220$ K and a local minimum point at approximately $T_2 = 300$ K, respectively. Below, in the reverse transition voltage versus temperature plot, the thermionic current is larger than the tunneling one, while above it the tunneling current is larger than the thermionic emission one. Appearance of the peak at low temperatures means that thermionic emission mechanism is preponderant in this range of low temperatures. This new behavior is not expected by the Padovani–Stratton model (Eq. (10)).

The increase in the reverse transition voltage for low (< T_1) and high temperatures (> T_2) means that the emission current component is larger than the tunneling current component, when the temperature is increased, and in order for these two current components to be equal, the current tunneling component should be increased by increasing the reverse bias, and *vice versa* when the reverse transition voltage decreases within the ranges of intermediate temperatures ($T_1 < T < T_2$) [26].

The influence of doping concentration on reverse transition voltage as a function of temperature is shown in Fig. 3. As shown in this figure, the reverse transition voltage increases with decreasing the doping concentration due to the decrease in the tunneling probability, because electrons see a thick barrier. The tw o temperatures T_1 and T_2 that correspond to the local maximum and minimum, respectively, do not vary with the doping concentration. As shown in the inset to Fig. 3, for a fixed temperature, the reverse transition voltage increases linearly with the inverse of doping concentration (N_D^{-1}).

Fig. 4 shows the influence of barrier height on reverse transition voltage as a function of temperature for β-Ga_2O_3 SBD. The temperatures T_1 and T_2 corresponding to the local extrema increase linearly with increasing the barrier height in accord to the following equations: $T_1 = 20 + 200\phi_b$ for T_1 and $T_2 = 300\phi_b$ for T_2.

For a given temperature (T_2^*), the reverse transition voltage remains unchangeable until the barrier height reaches the value (ϕ_b^*), from which the local minimum occurs at the same temperature (T_2^*). For example, when the barrier height is $\phi_b^* = 1$ eV, the local minimum occurs at $T_2^* = 300$ K, as shown in Fig. 4. Above the barrier height ϕ_b^* the reverse transition voltage increases linearly

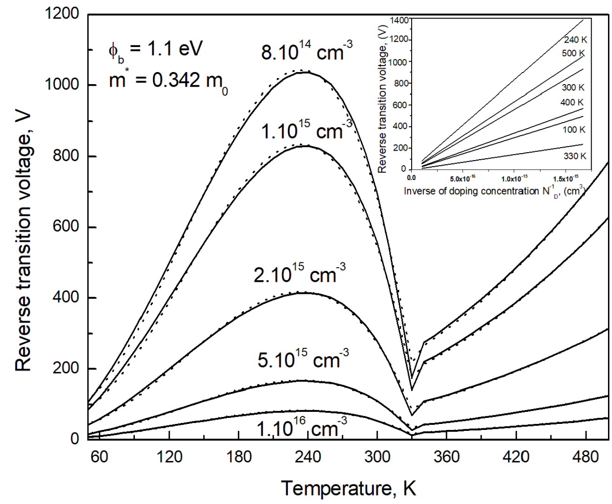

Fig. 3. Reverse transition voltage *versus* temperature plot for various doping concentrations for β-Ga_2O_3 SBD. The dotted lines are the curves fitted by using our proposed model (Eqs. (14) and (15)). The inset shows the reverse transition voltage as a function of the inverse doping concentration for various temperatures.

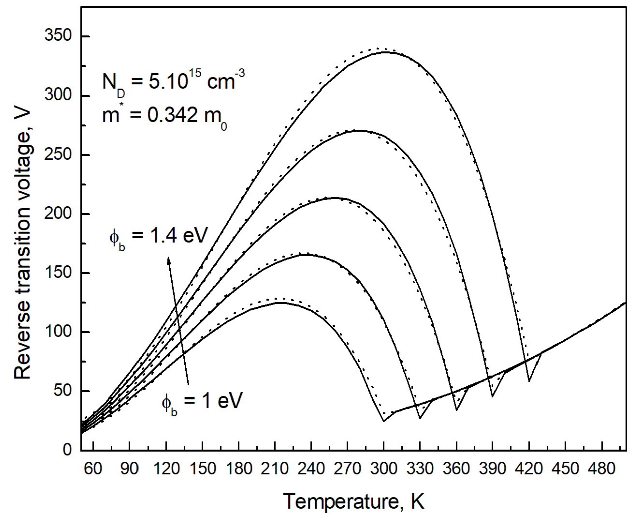

Fig. 4. Reverse transition voltage *versus* temperature plot for various barrier heights for β-Ga_2O_3 SBD. The dotted lines are the curves fitted by using our proposed model (Eqs. (14) and (15)).

with increasing the barrier height as shown in Fig. 5 for various temperatures within the range 270…390 K with the step 30 K. When the barrier height is below ϕ_b^*, the amount of decrease of both these current components is of the same order of magnitude, while, when the barrier height reaches ϕ_b^*, the tunneling current component decreases faster than the thermionic emission current, as shown in the inset to Fig. 5.

By fitting several simulated data of reverse transition voltage as a function of temperature and barrier height, with the parameters: $A^* = 41.1$ A cm^{-2}·K^{-2}, $m^* = 0.342m_0$ and $\varepsilon_s = 10.2\varepsilon_0$, and by following the same

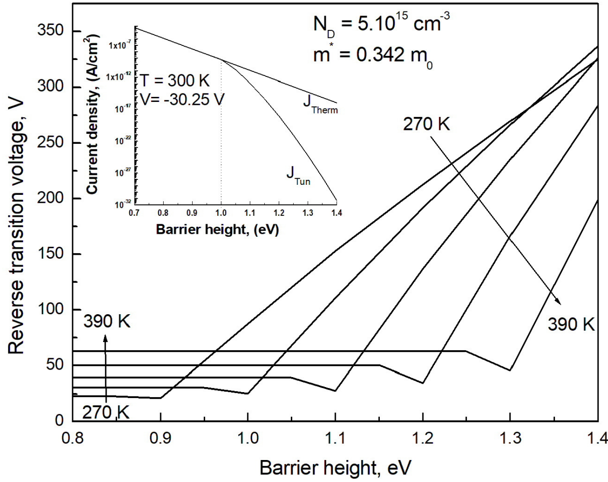

Fig. 5. Reverse transition voltage as a function of barrier height for various temperatures for β-Ga_2O_3 SBD. The inset shows the current densities J_{Tun} and J_{Therm} *versus* barrier height at 300 K and $V = -30.25$ V.

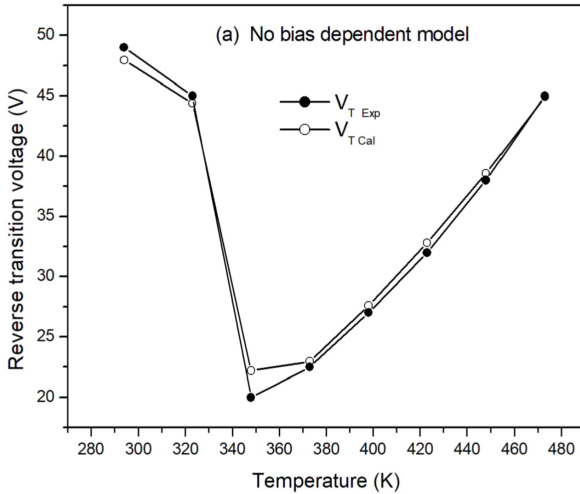

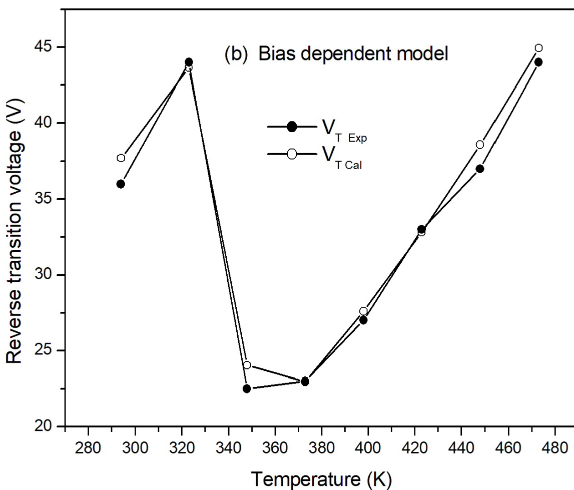

Fig. 6. Comparison between experimental reverse transition voltages and those calculated using our model (Eqs. (14) and (15)) for β-Ga_2O_3 SBD. (a) $V_{T\,Exp}$ obtained using the no bias dependence of the barrier height model [39], (b) $V_{T\,Exp}$ obtained using the bias dependence of the barrier height model [40].

steps outlined in our previous work [26], the following function relationships can be obtained for β-Ga_2O_3 SBD:

$$V_T \approx \begin{cases} \left[f(\phi_b) + g(\phi_b)T + h(\phi_b)T^2 + p(\phi_b)T^3\right]\left(\frac{10^{15}}{N_D}\right), \\ 50\,\mathrm{K} \le T \le T_2 = 300\phi_b \\ \left[262.349 - 2.016T + 5.5\cdot 10^{-3}T^2\right]\left(\frac{10^{15}}{N_D}\right), \\ T \succ T_2 = 300\phi_b. \end{cases} \quad (14)$$

Here, the functions $f(\phi_b)$, $g(\phi_b)$, $h(\phi_b)$, and $p(\phi_b)$ are linearly dependent on the barrier height and given by

$$\begin{cases} f(\phi_b) = -107.9 + 199.642\phi_b \\ g(\phi_b) = (0.458 - 3.565\phi_b) \\ h(\phi_b) = (21.8 + 43.25\phi_b)10^{-3} \\ p(\phi_b) = (-210.41 + 30.63\phi_b)10^{-6} \end{cases} \quad (15)$$

Using this model, we can predict the reverse transition voltage between the thermionic emission and tunneling mechanisms for any temperature range and reverse bias range; therefore, we can know which conduction mechanism is appropriate for analysis of the experimental data for β-Ga_2O_3 SBDs. As shown in Figs. 3 and 4, our proposed analytical model indicated by the dotted lines is in good agreement with the simulated data. Moreover, in order to validate our proposed model, we tested it on experimental data previously published in the literature [40]. As shown in Fig. 6, the reverse transition voltage calculated using our model is in a good agreement with the experimental reverse transition voltage, whether for the experimental data obtained by the no bias dependence of the barrier height model (Fig. 6a) or for those obtained by the bias dependence of the barrier height model (Fig. 6b).

4. Conclusions

In this study, we have applied the theoretical method to investigate the conduction mechanisms of the leakage current of β-Ga_2O_3 SBDs, which allow us to determine the ranges of temperature and reverse bias, over which β-Ga_2O_3 Schottky diodes exhibit tunneling and thermionic emission in the case when the image force lowering is included. This method has been applied due to equality between the tunneling and thermionic emission current components of the total current. Unexpected peak by Padovani–Stratton's condition is observed in the reverse transition voltage *versus* temperature curve at low temperatures, which means that the thermionic emission mechanism is preponderant in this range of low temperatures. In order to predict the reverse transition voltage between both these mechanisms as a function of temperature, barrier height and doping concentration, an analytical model has been proposed. Experimental reverse transition voltage data previously published in the literature are well described by our model.

References

1. Zhang Z., Farzana E., Arehart A.R. and Ringel S.A. Deep level defects throughout the bandgap of (010) β-Ga_2O_3 detected by optically and thermally stimulated defect spectroscopy. *Appl. Phys. Lett.* 2016. **108**. P. 052105. https://doi.org/10.1063/1.4941429.
2. Higashiwaki M., Sasaki K., Kuramata A., Masui T. and Yamakoshi S. Gallium oxide (Ga_2O_3) metal-semiconductor field-effect transistors on single-crystal β-Ga_2O_3 (010) substrates. *Appl. Phys. Lett.* 2012. **100**. P. 013504. https://doi.org/10.1063/1.3674287.
3. Fujita S. Wide-bandgap semiconductor materials: For their full bloom. *Jpn. J. Appl. Phys. Part 1*. 2015. **54**. P. 030101. https://doi.org/10.7567/JJAP.54.030101.
4. Stepanov S.I., Nikolaev V.I., Bougrov V.E. and Romanov A.E. Gallium oxide: properties and applications – a review. *Rev. Adv. Matter. Sci.* 2016. **44**. P. 63–86.
5. Pearton S.J., Jiancheng Yang J., Cary P.H. *et al*. A review of Ga_2O_3 materials, processing, and devices. *Appl. Phys. Rev*. 2018. **5**. P. 011301. https://doi.org/10.1063/1.5006941.
6. Víllora E.G., Arjoca S., Shimamura K., Inomata D., and Aoki K. β-Ga_2O_3 and single-crystal phosphors for high-brightness white LEDs & LDs, and β-Ga_2O_3 potential for next generation of power devices. *Proc SPIE*, Oxide-based Materials and Devices. 2014. **8987**. P. 89871U. https://doi.org/10.1117/12.2039305.
7. Kaun S.W., Wu F. and Speck J.S. β-$(Al_xGa_{1-x})_2O_3$/ Ga_2O_3 (010) heterostructures grown on β-Ga_2O_3 (010) substrates by plasma-assisted molecular beam epitaxy. *J. Vac. Sci. Technol. A*. 2015. **33**. P. 041508. https://doi.org/10.1116/1.4922340.
8. Sasaki K., Higashiwaki M., Kuramata A., Masui T. and Yamakoshi S. Ga_2O_3 Schottky barrier diodes fabricated by using single-crystal β–Ga_2O_3 (010) substrate. *IEEE Electron. Device Lett*. 2013. **34**. P. 493–495. https://doi.org/10.1109/LED.2013.2244057.
9. Oishi T., Koga Y., Harada K. and Kasu M. High-mobility β-Ga_2O_3 (201) single crystals grown by edge-defined film-fed growth method and their Schottky barrier diodes with Ni contact. *Appl. Phys. Express*. 2015. **8**. P. 031101. https://doi.org/10.7567/APEX.8.031101.
10. Jayawardena A., Ahyi A.C. and Dhar S. Analysis of temperature dependent forward characteristics of Ni/$(\bar{2}01)$ β-Ga_2O_3 Schottky diodes. *Semicond. Sci. Technol*. 2016. **31**. P. 115002. https://doi.org/10.1088/0268-1242/31/11/115002.
11. Higashiwaki M., Sasaki K., Murakami H. *et al*. Recent progress in Ga_2O_3 power devices. *Semicond. Sci. Technol*. 2016. **31**. P. 034001. https://doi.org/10.1088/0268-1242/31/3/034001
12. Higashiwaki M., Konishi K., Sasaki K. *et al*. Temperature-dependent capacitance–voltage and current–voltage characteristics of Pt/Ga_2O_3 (001) Schottky barrier diodes fabricated on *n*–Ga_2O_3 drift layers grown by halide vapor phase epitaxy. *Appl. Phys. Lett*. 2016. **108**. P. 133503. https://doi.org/10.1063/1.4945267.
13. Oh S., Yang G. and Kim J. Electrical characteristics of vertical Ni/β-Ga_2O_3 Schottky barrier diodes at high temperatures. *ECS J. Solid State Sci. Technol*. 2017. **6**. P. Q3022. https://doi.org/10.1149/2.0041702jss.
14. Yao Y., Gangireddy R., Kim J., Das K.K., Davis R. F. and Porter L.M. Electrical behavior of β-Ga_2O_3 Schottky diodes with different Schottky metals. *J. Vac. Sci. Technol. B*. 2017. **35**. P. 03D113. https://doi.org/10.1116/1.4980042.
15. Ahmadi E., Oshima Y., Wu F. and Speck J.S. Schottky barrier height of Ni to β-$(Al_xGa_{1-x})_2O_3$ with different compositions grown by plasma-assisted molecular beam epitaxy. *Semicond. Sci. Technol*. 2017. **32**. P. 035004. https://doi.org/10.1088/1361-6641/aa53a7.
16. Farzana E., Zhang Z., Paul P.K., Arehart A.R. and Ringel S.A. Influence of metal choice on (010) β-Ga_2O_3 Schottky diode properties. *Appl. Phys. Lett*. 2017. **110**. P. 20210. https://doi.org/10.1063/1.4983610.
17. He Q., Mu W., Dong H., Long S., Jia Z., Liu H.L.Q. , Tang M., Tao X., and Liu M. Schottky barrier diode based on β-Ga_2O_3 (100) single crystal substrate and its temperature-dependent electrical characteristics. *Appl. Phys. Lett*. 2017. **110**. P. 093503. https://doi.org/10.1063/1.4977766.
18. Konishi K., Goto K., Murakami H., Kumagai Y., Kuramata A., Yamakoshi S. and Higashiwaki M. 1-kV vertical Ga_2O_3 field-plated Schottky barrier diodes. *Appl. Phys. Lett.* 2017. **110**. P. 103506. https://doi.org/10.1063/1.4977857.
19. Oshima T., Hashiguchi A., Moribayashi M. *et al.* Electrical properties of Schottky barrier diodes fabricated on (001) β-Ga_2O_3 substrates with crystal defects. *Jpn. J. Appl. Phys*. 2017. **56**. P.086501. https://doi.org/10.7567/JJAP.56.086501
20. Yang J., Ren F., Khanna R. *et al.* Annealing of dry etch damage in metallized and bare $(\bar{2}01)$ Ga_2O_3. *J. Vac. Sci. Technol. B*. 2017. **35**. P. 051201. https://doi.org/10.1116/1.4986300.
21. Li A., Feng Q., Zhang J., Hu Z. *et al*. Investigation of temperature dependent electrical characteristics on Au/Ni/β-Ga_2O_3 Schottky diodes. *Superlattices and Microstructures*. 2018. **119**. P. 212–217. https://doi.org/10.1016/j.spmi.2018.04.045.
22. He Q., Mu W., Fu B., Jia Z. *et al*. Schottky barrier rectifier based on (100) β-Ga_2O_3 and its DC and AC characteristics. *IEEE Electron Device Letters*. 2018. **39**. P. 556–559. https://doi.org/10.1109/LED.2018.2810858.
23. Jian G., He Q., Mu W., Fu B. *et al*. Characterization of the inhomogeneous barrier distribution in a Pt/(100) β–Ga_2O_3 Schottky diode via its temperature-dependent electrical properties. *AIP Advances*.

2018. **8**. P. 015316.
https://doi.org/10.1063/1.5007197.

24. Fu H., Chen H., Huang X., Baranowski I. *et al*. A comparative study on the electrical properties of vertical ($\bar{2}01$) and (010) β-Ga_2O_3 Schottky barrier diodes on EFG single-crystal substrates. *IEEE Trans. on Electron Devices*. 2018. **65**. P. 3507–3513. https://doi.org/10.1109/TED.2018.2841904.
25. Yang J., Ren F., Tadjer M., Pearton S.J., and Kuramata A. Ga_2O_3 Schottky rectifiers with 1 ampere forward current, 650 V reverse breakdown and 26.5 MW·cm^{-2} figure-of-merit. *AIP Advances*. 2018. **8**. P. 055026. https://doi.org/10.1063/1.5034444.
26. Latreche A. Conduction mechanisms of the reverse leakage current of 4H-SiC Schottky barrier diodes. *Semicond. Sci. Technol*. 2019. **34**. P. 025016. https://doi.org/10.1088/1361-6641/aaf8cb.
27. Latreche A. Combination of thermionic emission and tunneling mechanisms to analyze the leakage current in 4H-SiC Schottky barrier diodes. *Semiconductor Physics, Quantum Electronics and Optoelectronics*. 2019. **22**. P. 19–25. https://doi.org/10.15407/spqeo22.01.20.
28. Chang C.Y., and Sze S.M. Carrier transport across metal-semiconductor barriers. *Solid-State Electron*. 1970. **13**. P. 727–740. https://doi.org/10.1016/0038-1101(70)90060-2.
29. Furno M., Bonani F. and Ghione G. Transfer matrix method modelling of inhomogeneous Schottky barrier diodes on silicon carbide. *Solid-State Electron*. 2007. **51**. P. 466–474. https://doi.org/10.1016/j.sse.2007.01.028.
30. Rhoderick E.H. and Williams R.H. *Metal–Semiconductor Contact*. Oxford: Oxford University Press, 1988.
31. Eriksson J., Rorsman N. and Zirath H. 4H-silicon carbide Schottky barrier diodes for microwave applications. *IEEE Trans. Microwave Theory Technol*. 2003. **51**. P. 796–804. https://doi.org/10.1109/TMTT.2003.808610.
32. Tsu R. and Esaki L. Tunneling in a finite superlattice. *Appl. Phys. Lett*. 1973. **22**. P. 562–564. https://doi.org/10.1063/1.1654509.
33. Latreche A. and Ouennoughi Z. Modified Airy function method modeling of tunnelling current for Schottky barrier diodes on silicon carbide. *Semicond. Sci. Technol*. 2013. **28**. P. 105003. https://doi.org/10.1088/0268-1242/28/10/105003.
34. Zheng L., Joshi R.P. and Fazi C. Effects of barrier height fluctuations and electron tunnelling on the reverse characteristics of 6H–SiC Schottky contacts. *J. Appl. Phys*. 1999. **85**. P. 3701–3707. https://doi.org/10.1063/1.369735.
35. Padovani F.A. and Stratton R. Field and thermionic-field emission in Schottky barriers. *Solid-State Electron*. 1962. **9**. P. 695–707. https://doi.org/10.1016/0038-1101(66)90097-9.
36. Latreche A. Validity of the Padovani–Stratton formulas for analysis of reverse current–voltage characteristics of 4H–SiC Schottky barrier diodes. *Semicond. Sci. Technol*. 2019. **34**. P. 055021. https://doi.org/10.1088/1361-6641/ab1191.
37. He H., Orlando R., Blanco M.A. and Pandey R. First-principles study of the structural, electronic, and optical properties of Ga_2O_3 in its monoclinic and hexagonal phases. *Phys. Rev. B*. 2006. **74**. P. 195123. https://doi.org/10.1103/PhysRevB.74.195123.
38. Hoeneisen B., Mead C.A. and Nicolet M.A. Permittivity of β-Ga_2O_3 at low frequencies. *Solid-State Electron*. 1971. **14**. P. 1057–1059. https://doi.org/10.1016/0038-1101(71)90176-6.
39. Passlack M., Hunt N.E.J., Schubert E.F., Zydzik G.J ., Hong M., Mannaerts J.P., Opila R.L. and Fischer R.J. Dielectric properties of electron-beam deposited Ga_2O_3 films. *Appl. Phys. Lett*. 1994. **64**. P. 2715–2717. https://doi.org/10.1063/1.111452.
40. Latreche A. Combined thermionic emission and tunneling mechanisms for the analysis of the leakage current for Ga_2O_3 Schottky barrier diodes. *SN Appl. Sci*. 2019. **1**. P. 188. https://doi.org/10.1007/s42452-019-0192-2.

Authors and CV

Abdelhakim Latreche is an assistant professor of the Department Material Sciences at Bordj Bou Arreridj University, Algeria. His main research interests include the electrical characterization and simulation of semiconductor devices, in particulary, wide gap (SiC, Ga_2O_3, ...) Schottky barrier diodes.